

Massively Parallel Mesoscopic Simulations of Gas Permeability of Thin Films Composed of Carbon Nanotubes

Alexey N. Volkov and Leonid V. Zhigilei

Abstract A mesoscopic computational model for simulation of gas flow through carbon nanotube (CNT) films is developed. The model is implemented in a parallel computational code enabling massively parallel dynamic simulations of CNT materials at length scales relevant to experimental studies. Self-diffusivity of Ar within CNT films with 9% volume fraction of the nanotubes and the effective diffusivity of Ar through the films are calculated for two different structures of the films: a continuous network of CNT bundles and a layered arrangement of dispersed individual CNTs. The results of the simulations suggest a moderate structural sensitivity of the gas diffusivity, with about 3–4.5 times lower values of self-diffusivity predicted for films with dispersed CNTs, and a smaller difference in the values of the effective diffusivity that are found to be on the order of $10^{-6} \text{ m}^2 \text{s}^{-1}$ for both film structures.

1 Introduction

Unique mechanical, thermal, and electrical properties of carbon nanotubes (CNTs) provide opportunities for their application as a component in novel multifunctional materials. The porous structure of CNT films or “buckypaper” also suggests a potential use of these materials in gas separation and storage. The design and optimization of new CNT-based materials can be facilitated by computational modeling of their mechanical, transport, and gas permeability properties. Computational studies of the effective properties of CNT-based materials, however, have been limited by the absence of models capable of describing large systems of interacting CNTs. Recent development of a mesoscopic dynamic model for CNT materials [11, 13, 16] opens up new opportunities for investigation of the structural dependence of various properties of this promising class of materials. In particular, first application of the mesoscopic model for analysis of thermal properties of buckypaper has revealed a

A.N. Volkov (✉)

Department of Materials Science and Engineering, University of Virginia, Charlottesville,
VA 22904-4745, USA
e-mail: av4h@virginia.edu

strong effect of self-organization of CNTs into a network of bundles on the effective thermal conductivity of the material [14]. In this paper we report an extension of the mesoscopic model to investigation of gas flow through thin CNT films and analysis of the connections between the film structure and gas permeability.

2 Mesoscopic Model for Dynamic Simulations and Structural Characterization of CNT Materials

In the mesoscopic model, every individual CNT is represented as a sequence of stretchable cylindrical segments [16]. Forces applied to the ends of the segments are described by a mesoscopic force field (MFF). The internal part of the MFF accounts for stretching and bending of CNTs [16]. Interactions between CNTs in MFF are described by the tubular potential method [11] based on the approximate inter-tube (tubular) potential [13]. The model is implemented in a parallel computational code designed to ensure a good scalability for massively parallel simulations.

In buckypaper and CNT films, individual nanotubes are arranged into continuous networks of interconnected bundles [10, 15]. These structures can be produced in mesoscopic dynamic simulations, in which initial samples with straight CNTs dispersed within layers stacked on top of each other, Fig. 1a, quickly (within several ns) evolve into steady-state random networks of interconnected CNT bundles, Fig. 1b [12, 13]. In order to study the effect of the structural arrangement of CNTs on the gas permeability of the CNT films, we perform simulations for Sample I with layered dispersed CNTs shown in Fig. 1a and Sample II with continuous network of CNT

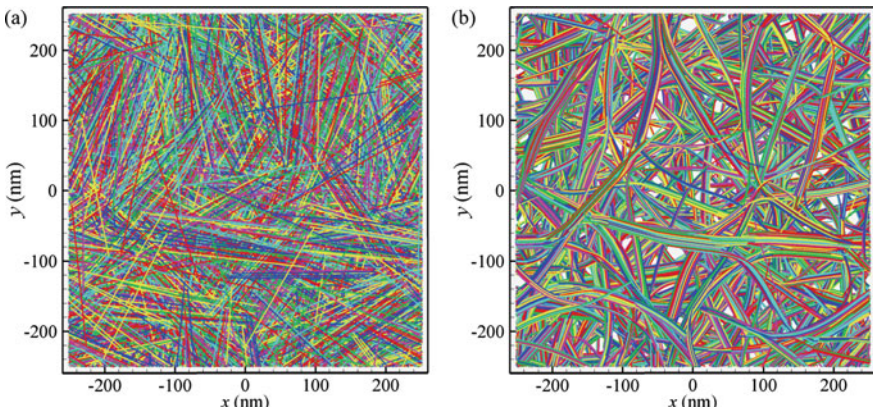


Fig. 1 Distributions of individual nanotubes in the initial Sample I composed of dispersed straight CNTs arranged into layers (a) and in Sample II obtained after 6 ns of dynamic mesoscopic simulation that resulted in the formation of a stable continuous network of bundles (b). The samples are composed of 7,829 (10,10) single-walled CNTs with radius $R_T = 0.6785$ nm. The length of each CNT is 200 nm, the dimensions of the systems are $500\text{ nm} \times 500\text{ nm} \times 100\text{ nm}$, density of the material is 0.2 g cm^{-3} and porosity is 91%. Periodic boundary conditions are applied in x - and y -directions

bundles shown in Fig. 1b. Both samples are anisotropic films with preferred orientation of CNTs within the plane of the film and have the same density and porosity. The porous structures of the samples, however, are quite different, Fig. 2, with much smaller sizes of the pores present in Sample I. The most probable pore diameter of 23 nm in Sample II is in a good agreement with experimental value of 21 nm measured for SWCNT buckypaper [5]. Other structural characteristics of Sample II, e.g., average bundle diameter, also agree with experimental observations [10, 15].

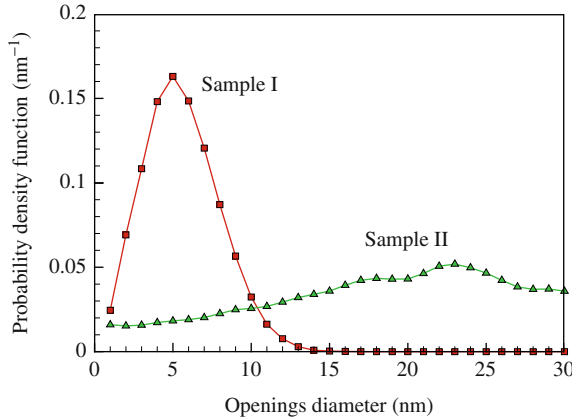


Fig. 2 Probability density function of opening diameters calculated in granulometric analysis of digitized CNT samples I (square symbols, Fig. 1a) and II (triangular symbols, Fig. 1b) with a voxel size of 0.5 nm. Distributions are not calculated for opening diameters larger than 30 nm due to the limited thickness of the CNT films

3 Mesoscopic Model for Gas-CNT Systems

In the mesoscopic model used in the simulations of gas flow through a CNT material, motion of individual gas atoms is described by equations of motion similar to those of conventional molecular dynamics method [2]. Assuming that CNTs are not movable and form a rigid porous network, the forces experienced by the gas atoms are defined by the following potential:

$$U = \sum_{i=1}^N \sum_{j=i+1}^N \varphi_{gg}(r_{ij}) + \sum_{i=1}^N \sum_{k=1}^M U_{CNT(i,k)}, \quad (1)$$

where $\varphi_{gg}(r_{ij})$ is the Lennard-Jones potential describing the interaction between gas atoms i and j separated by a distance of r_{ij} , $U_{CNT(i,k)}$ is a mesoscopic potential for interaction between gas atom i and CNT k , N and M are the total numbers of gas atoms and CNTs, respectively. The potential $\varphi_{gg}(r_{ij})$ is parameterized for Argon atoms [1, 8] and a cubic cutoff function [13] is used to smoothly bring the potential to zero at $r_{ij} = 11.9 \text{ \AA}$.

For a gas atom – CNT pair, the corresponding interaction potential $U_{CNT(ik)}$ is calculated based on potential $U_{CNT\infty}$ describing the interaction between an atom and a straight infinitely long nanotube, Fig. 3a. This potential depends only on the shortest distance r_S from the atom to the surface of the nanotube and can be calculated as follows

$$U_{CNT\infty}(r_S) = 4n_\sigma R_T \int_0^{+\infty} \int_0^\pi \varphi_{gc} \left(\sqrt{x^2 + (R_T(1 - \cos \phi) + r)^2 + R_T^2 \sin^2 \phi} \right) d\phi dx, \quad (2)$$

where $\varphi_{gc}(r)$ is the interaction potential between a gas atom and a carbon atom on the surface of the CNT separated by interatomic distance r , R_T is the radius of the CNT, n_σ is the surface density of carbon atoms on the surface of the CNT, and the distance x and angle ϕ are defined as shown in Fig. 3a. The potential $\varphi_{gc}(r)$ is adopted in the form of the Lennard-Jones potential with a cubic spline cutoff function [13] and parameterized for interaction between C and Ar atoms [1, 8]. The values of $U_{CNT\infty}$ and its derivative are calculated numerically and used in a tabulated form in the simulations.

The description of the interaction between a gas atom and a curved CNT is based on representation of the nanotube by a chain of cylindrical segments with spherical junctions between them and semispherical caps at the nanotube ends, Fig. 3b. For each of the gas atoms, a list of the nanotube elements (segments, junctions, or caps) with surfaces that are within the potential cutoff distance r_c from the atom is formed. Segments are included in this list only if the points on their axes closest to the atom are within the segment, e.g., point D_1 for atom D and segment 1 in Fig. 3b. The length of the segments is chosen to be larger than r_c and, in cases shown in Fig. 3b for atoms A , B , and C , this list contains no more than one segment of the nanotube. In these cases, $U_{CNT(ik)} = U_{CNT\infty}(r_{\min})$, where r_{\min} is the closest distance to the

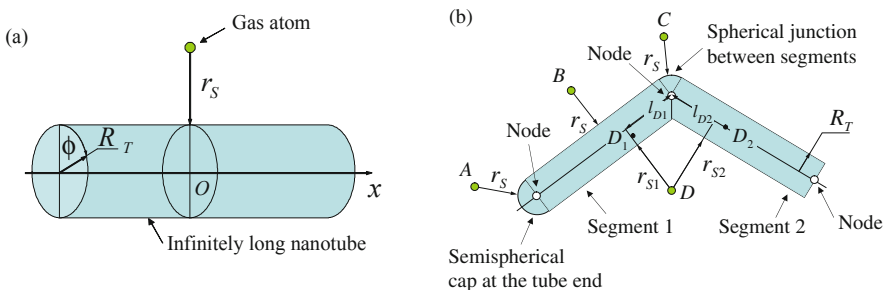


Fig. 3 Schematic drawings illustrating the interaction between a gas atom and a straight infinitely long CNT of radius R_T (a) and between a gas atom and a part of a CNT consisting of a semispherical cap on the nanotube end, two segments, and a spherical junction between them (b). In panel (b), letters A, B, C, and D indicate various possible positions of gas atoms interacting with the nanotube

surfaces of the nanotube elements from the list. If the list contains several segments, then $U_{CNT(ik)}$ is calculated as a weighted sum of potentials for all segments in the list. For example, for atom D in Fig. 3b, the potential $U_{CNT(ik)}$ is calculated as $U_{CNT(ik)} = w_1 U_{CNT\infty}(r_{S1}) + w_2 U_{CNT\infty}(r_{S2})$, where $w_m = l_{Dm}/(l_{D1} + l_{D2})$ and l_{Dm} is the distance between the point D_m on the axis of the segment m ($m = 1, 2$) that is the closest point to the gas atom and the node joining segments 1 and 2. This approach can easily be adopted for interactions of gas atoms with more than two segments of a highly curved CNT.

4 Gas Self-Diffusivity Within CNT Films

The computational setup for simulations of self-diffusivity of argon atoms within CNT films is shown in Fig. 4a. The films, generated without periodic boundary condition in z (out of plane) direction, are immersed into a gas reservoir with small gaps of thickness δ between the film surfaces and the reservoir boundaries. The periodic boundary conditions are then imposed in all three directions and dynamic simulations of Ar gas equilibrated at a temperature of 300 K and different values of pressure are performed. The Ar self-diffusivities in the in-plane, D_x and D_y , and out-of-plane, D_z , directions are calculated with the Einstein relation [2],

$$D_\alpha = \lim_{t \rightarrow \infty} \frac{1}{2t} \left\langle \frac{1}{N} \sum_{i=1}^N |\alpha_i(t) - \alpha_i(0)|^2 \right\rangle, \quad (3)$$

where $\alpha = x, y, z$ and $\alpha_i(t)$ is the true (corrected to eliminate the effect of the periodic boundary conditions) α coordinate of Ar atom i at time t .

The self-diffusivity $D = (D_x + D_y + D_z)/3$ in pure Ar gas (without the presence of a CNT film) at a temperature of 273 K and pressure of 101325 Pa is found to be equal to $1.56 \times 10^{-5} \text{ m}^2 \text{s}^{-1}$, which is in a good agreement with experimental value

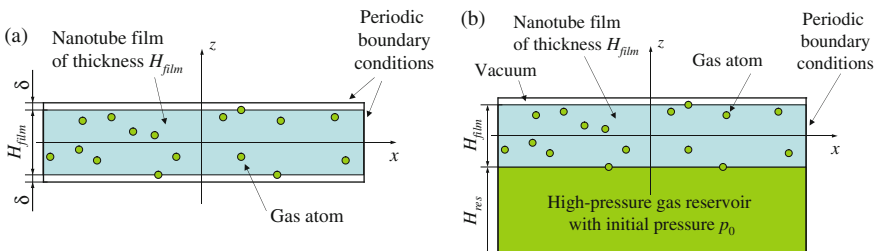


Fig. 4 Computational cell used in the simulations of self-diffusivity of gas atoms within a CNT film (a) and gas permeability through a CNT film from a high-pressure reservoir to vacuum (b). Periodic boundary conditions are imposed in all directions in (a) and in the lateral (parallel to the film surface) directions in (b)

of $1.57 \times 10^{-5} \text{ m}^2 \text{s}^{-1}$ [4]. The inverse proportionality of D to pressure (dashed lines in Fig. 5) also agrees with predictions of the kinetic theory of gases [4].

The mean free path of argon atoms at 0.1 bar is about 500 nm, much larger than the most probable diameter of openings revealed in the granulometric analysis of CNT samples (Fig. 2). Therefore, the Knudsen regime of gas flow through the porous CNT film is realized in simulations at pressure values below ~ 0.1 bar. Under these conditions, the collisions between the gas atoms and CNTs play the dominant role in defining the values of self-diffusivity, which can be expected to be independent on the gas pressure. The results of the simulations shown in Fig. 5 are consistent with this analysis. Moreover, in the range of partial gas pressure, p , up to 3 bars, the self-diffusivities of Ar exhibit only a weak tendency to decrease with increasing p . The presence of nanotubes reduces the self-diffusivity of argon in the out-of-plane direction more appreciably than in the in-plane direction (Fig. 5). The self-diffusivities exhibit moderate sensitivity to the film structure, with the values predicted for Sample II (network of bundles) being $\sim 3\text{--}4.5$ times larger than in Sample I (layered dispersed CNTs). For Sample I, which thickness, H_{film} , can be easily changed in simulations, no noticeable changes in the results are observed with increase of H_{film} .

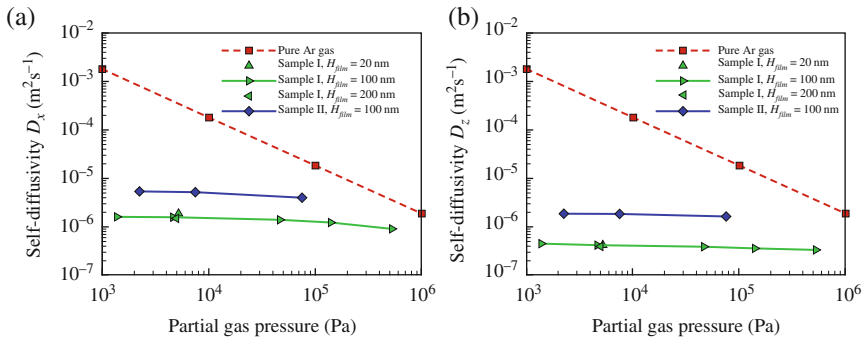


Fig. 5 The values of self-diffusivity of Ar in x - and z -directions, D_x (a) and D_z (b), predicted in simulations of Ar gas diffusion in Samples I and II shown in Fig. 1. The simulations are performed at temperature 300 K and various values of the partial gas pressure. The partial gas pressure is calculated based on the ideal gas equation $p = nkT$, where $n = N/V$ and T are the gas number density and temperature, k is the Boltzmann constant, N is the total number of Ar atoms, and V is the sample volume. *Dashed lines* correspond to the self-diffusivity obtained in simulations of pure Ar gas

5 Gas Permeability of CNT Films

The computational setup for simulations of gas permeability of CNT films shown in Fig. 4b mimics the experimental setups used for measurement of gas permeability of porous materials [6, 7, 9]. A CNT film is placed in between a high-pressure

reservoir with initial gas pressure p_0 and a vacuum reservoir, where the pressure is zero. The simulations are performed at a constant temperature of 300 K maintained by the Berendsen thermostat method [3]. Gas atoms gradually permeate through the film and the pressure in the high-pressure reservoir, $p(t)$, drops. Assuming that the size of the reservoir is sufficiently large and the normal diffusion (where the effective diffusivity is independent on pressure) is realized [6], the pressure decay, after completion of the initial filling of the film by the gas atoms (Fig. 6a), should be exponential, i.e. $p(t) = p(t_0) \exp(-(t - t_0)/\tau)$ [6, 9]. Once $p(t)$ is measured, one can use it for calculation of the time constant τ and, in turn, the effective gas diffusivity through the film, $D_{eff} = V_{res}H_{film}/(A_{film}\tau) = H_{res}H_{film}/\tau$ (Fig. 6b), where $V_{res} = H_{res}A_{film}$ and H_{res} are the volume and thickness of the gas reservoir, and A_{film} and H_{film} are the surface area and thickness of the film.

Fast convergence or D_{eff} with increasing H_{res} enables computationally efficient evaluation of the gas permeability of thin nanoporous films in the mesoscopic simulations. In particular, $H_{res} = 400$ nm is found to ensure a sufficiently accurate calculation of D_{eff} for samples I and II, with errors being within 5% with respect to further increase in H_{res} . The time t_0 , needed for the initial filling of the film depends on the effective diffusivity of the film and, hence, is larger for Sample I than for Sample II. With a proper choice of t_0 , the time dependence of D_{eff} exhibits only small variations around its averaged value caused by the finite thickness of the film (Fig. 6b). This observation suggests that the gas permeation occurs in the normal diffusion regime. The values of D_{eff} are found to be within 25% from the corresponding values of self-diffusivity D_z . The value of D_{eff} determined for sample I is ~ 3 times smaller than that for Sample II.

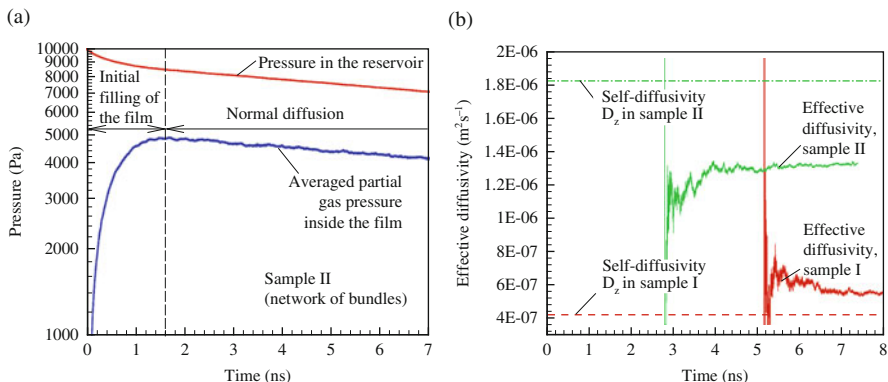


Fig. 6 Pressure in the high pressure reservoir and average partial gas pressure inside the film vs. time (a) and the effective diffusivity D_{eff} vs. time (b) in the gas permeation simulations. In panel (a), solid curves correspond to the pressure in the reservoir and inside the film obtained for Sample II. In panel (b), solid curves are obtained for samples I and II, dashed and dash-dotted lines correspond to the self-diffusivity D_z in samples I and II at a pressure of 0.1 bar. Simulations are performed with $H_{res} = 400$ nm, $p_0 = 10^4$ Pa, and temperature of 300 K. Time t_0 is chosen to be 5 ns for Sample I and 2.5 ns for Sample II

In [9], the effective diffusivity of a few common gases through films composed of dispersed multi-walled CNT was measured and values of D_{eff} for N₂ (kinetic diameter of N₂ gas at 300 K is close to that of Ar) and sufficiently thick samples were found to be in the range of $(7.2\text{--}8.2) \cdot 10^{-6} \text{ m}^2\text{s}^{-1}$ ¹. In order to compare the results of the mesoscopic simulations with these experiments, an additional Sample III was generated with basic properties that were similar to those in experimental samples. This sample of size 500 nm × 500 nm × 200 nm was composed of dispersed CNTs with external radius of 9.73 nm and length of 200 nm. The CNTs are arranged in parallel layers similar to those in Sample I. The density of Sample III, 0.31 g cm⁻³, was calculated assuming that every CNT has 23 walls with the radius of the internal wall equal to 2.25 nm. The volume fraction of CNTs was equal to 15%. The simulation of Ar permeation through Sample III, performed at 300 K with $H_{res} = 1,000$ nm and $p_0 = 10^4$ Pa, predicts $D_{eff} = 5.9 \cdot 10^{-6} \text{ m}^2\text{s}^{-1}$, which is within 20–30% from the experimental values. Based on the comparison of the results obtained for samples I and II, one can expect that the film composed of the multi-walled CNTs would have a somewhat higher effective diffusivity if the layered system of dispersed straight CNTs would be allowed to evolve in a dynamic mesoscopic simulation into a more realistic structure of interconnected network of CNT bundles with larger pore sizes as compared to layered systems of straight nanotubes.

6 Conclusion

Self-diffusivity of Ar gas within CNT films and the effective diffusivity of Ar gas through the films are studied in mesoscopic simulations. In permeation simulations, the pressure in the high-pressure reservoir follows the exponential dependence characteristic of the normal diffusion. The effective diffusivity is found to be of the same order of magnitude as the gas self-diffusivity in the direction perpendicular to the surface of the film. Simulations predict the effective diffusivities on the order of $10^{-6} \text{ m}^2\text{s}^{-1}$ for films with 9% volume fraction of (10,10) CNTs and a moderate sensitivity of the diffusivity on the film structure.

Acknowledgements The financial support is provided by AFOSR (Grant No FA9550-10-10545) and NSF (Grant No CBET-1033919). Computational support is provided by NCCS at ORNL (project MAT009). The authors would like to thank Dr. Akos Kukovecz of the University of Szeged, Hungary for helpful communication at the final stage of the paper preparation.

¹As clarified through communication with Dr. Akos Kukovecz, the values of the effective diffusivity reported in table 4 of [9] are given in units of mol s kg⁻¹ and not in units of m² s⁻¹ as erroneously stated in the paper. The values should be multiplied by a factor of RT (R is the universal gas constant, $T = 298$ K) to be converted to units of m² s⁻¹.

References

1. Ackerman, D.M., Skoulidas, A.I., Sholl, D.S., Johnson, J.K.: Diffusivities of Ar and Ne in carbon nanotubes. *Mol. Simul.* **29**, 677–684 (2003)
2. Allen, M.P., Tildesley, D.J.: Computer Simulation of Liquids. Clarendon Press, Oxford (1987)
3. Berendsen, H.J.C., Postma, J.P.M., van Gunsteren, W.F., DiNola, A., Haak, J.R.J.: Molecular dynamics with coupling to an external bath. *Chem. Phys.* **81**, 3684–3690 (1984)
4. Chapman, S., Cowling, T.G.: The Mathematical Theory of Non-uniform Gases. Cambridge University Press, Cambridge (1970)
5. Cinke, M., Li, J., Chen, B., Cassell, A., Delzeit, L., Han, J., Meyyappan, M.: Pore structure of raw and purified HiPco single-walled carbon nanotubes. *Chem. Phys. Lett.* **365**, 69–74 (2002)
6. Cooper, S.M., Chuang, H.F., Cinke, M., Cruden, B.A., Meyyappan, M.: Gas permeability of a buckypaper membrane. *Nano Lett.* **3**, 189–192 (2003)
7. Dullien, F.A.L.: Porous Media. Fluid Transport and Porous Structure. Academic Press, New York, NY (1979)
8. Skoulidas, A.I., Sholl, D.S.: Transport diffusivities of CH₄, CF₄, He, Ne, Ar, Xe, and SF₆ in silicalite from atomistic simulations. *J. Phys. Chem. B* **106**, 5058–5067 (2002)
9. Smajda, R., Kukovecz, Á., Kónya, Z., Kiricsi, I.: Structure and gas permeability of multi-wall carbon nanotube buckypapers. *Carbon* **45**, 1176–1184 (2007)
10. Thess, A., Lee, R., Nikolaev, P., Dai, H., Petit, P., Robert, J., Xu, C., Lee, Y.H., Kim, S.G., Rinzler, A.G., Colbert, D.T., Scuseria, G.E., Tománek, D., Fischer, J.E., Smalley, R.E.: Crystalline ropes of metallic carbon nanotubes. *Science* **273**, 483–487 (1996)
11. Volkov, A.N., Simov, K.R., Zhigilei, L.V.: Mesoscopic model for simulation of CNT-based materials. In: Proceedings of the ASME International Mechanical Engineering Congress and Exposition, ASME paper IMECE2008-68021 (2008)
12. Volkov, A.N., Simov, K.R., Zhigilei, L.V.: Mesoscopic simulation of self-assembly of carbon nanotubes into a network of bundles. In: Proceedings of the 47th AIAA Aerospace Sciences Meeting, AIAA paper 2009-1544 (2009)
13. Volkov, A.N., Zhigilei, L.V.: Mesoscopic interaction potential for carbon nanotubes of arbitrary length and orientation. *J. Phys. Chem. C* **114**, 5513–5531 (2010)
14. Volkov, A.N., Zhigilei, L.V.: Scaling laws and mesoscopic modeling of thermal conductivity in carbon nanotube materials. *Phys. Rev. Lett.* **104**, 215902 (2010)
15. Wang, S., Liang, Z., Wang, B., Zhang, C.: High-strength and multifunctional macroscopic fabric of single-walled carbon nanotubes. *Adv. Mater.* **19**, 1257–1261 (2007)
16. Zhigilei, L.V., Wei, C., Srivastava, D.: Mesoscopic model for dynamic simulations of carbon nanotubes. *Phys. Rev. B* **71**, 165417 (2005)